# Oxidative Decomposition of Methanol on Subnanometer Palladium Clusters: The Effect of Catalyst Size and Support Composition

**Sungsik Lee,[$,†] Byeongdu Lee,[‡] Faisal Mehmood,[§] Sönke Seifert,[‡] Joseph A. Libera,[||] Jeffrey W. Elam, Jeffrey Greeley,[⊥] Peter Zapol,[§] Larry A. Curtiss,[§,⊥] Michael J. Pellin,[§] Peter C. Stair,[†,#] Randall E. Winans,[‡] and Stefan Vajda[+,*,†,⊥,¶]**

*Chemical Sciences and Engineering Division, X-ray Sciences Division, Materials Science Division, Energy Systems Division, and Center for Nanoscale Materials, Argonne National Laboratory, 9700 South Cass Avenue, Argonne, Illinois 60439, Department of Chemistry, Northwestern University, 2145 Sheridan Road, Evanston, Illinois 60208, and Department of Chemical Engineering, School of Engineering & Applied Science, Yale University, 9 Hillhouse Avenue, New Haven, Connecticut 06520*

*Received: December 28, 2009; Revised Manuscript Received: May 2, 2010*

Size and support effects in the oxidative decomposition of methanol on amorphous alumina supported subnanometer palladium clusters were studied under realistic reaction conditions of pressure and temperature. The smaller $Pd_{8-12}$ clusters were found to promote the decomposition channel to CO and hydrogen, however with mediocre activity due to poisoning. The larger $Pd_{15-18}$ clusters preferentially produce dimethyl ether and formaldehyde, without signs of posioning. A thin titania overcoat applied on the $Pd_{15-18}$ improves the sintering-resistance of the catalyst. Accompanying density functional calculations confirm the posioning of small Pd clusters by CO.

## Introduction

Methanol plays an important role as an intermediate product in the chemical industry and also as an attractive, clean, and reliable future energy carrier. Palladium-based catalysts have been found to be very effective for the decomposition of methanol.[1−14] Decomposition, reforming, and partial oxidation of methanol, as well as their combination with water-gas shift (i.e., oxidative reforming) is attracting increasing attention because of the possibility of using methanol as a source of hydrogen for fuel cells.[15]

Methanol can be decomposed via various reaction pathways, involving the scission of the C−H, O−H, and C−O bonds. The latter channel may also lead to carbon deposits on the catalyst surface. Under UHV conditions, C−O bond scission does not occur on Pd (111) terraces, while under high-pressure conditions the C−O bond scission becomes favorable especially on specific active sites, leading to the formation of carbonaceous species that cause catalyst deactivation. Oxygen was found to enhance catalytic activity by more effective removal of the carbon deposits in the form of carbon oxides.[14]

While Pd surfaces and nanoparticles have been extensively studied for this reaction,[2,12,14,16] no studies of methanol activation have been reported for subnanometer Pd clusters. The studies of such well-defined ultrasmall clusters have been hampered by the lack of synthesis and in situ characterization methods. Recent breakthroughs in this area have shown that size-preselected subnanometer clusters can be fabricated and stabilized[17−19] and their catalytic properties studied over a broad pressure range.[18−22]

In this work, we fabricated a set of palladium catalysts by the deposition of size-selected subnanometer palladium clusters of two narrow size distributions, $Pd_{8-12}$ and $Pd_{15-18}$, on amorphous alumina supports. One cluster sample was post-treated by overcoating with titania with the twin goals to suppress sintering of clusters at elevated reaction temperatures and to alter the composition of the support. A combination of temperature programmed reaction (TPRx) with in situ grazing incidence small-angle X-ray scattering (GISAXS) was used to monitor catalytic activity of the supported clusters and for the simultaneous monitoring of particle size under reaction conditions.[19,23] Density functional calculations were used to investigate possible CO poisoning on the smaller clusters. The objective of the research is to improve, by using model catalytic structures, the fundamental understanding of size/composition/structure/function relationships in the activation of methanol.

## Experimental Section

**Support Material.** As catalyst support material, we used a 3 ML thin amorphous alumina film prepared by atomic layer deposition (ALD) on the top of a naturally oxidized silicon wafer ($SiO_2$/Si(100)). The silicon substrates were coated with $Al_2O_3$ using atomic layer deposition[24] in a custom viscous flow ALD reactor.[25] After equilibrating the reactor at 200 °C, 1 Torr pressure, and 360 sccm flow of ultrahigh purity (UHP, 99.999%) nitrogen for 10 min, the substrates were cleaned in situ, using a 400 sccm flow of 10% ozone in UHP oxygen for 1 min. The $Al_2O_3$ ALD was performed by using 6 ALD cycles consisting of a 2 s exposure to trimethylaluminum, a 5 s purge, a 2 s exposure to $H_2O$ vapor, and a final 5 s purge.[26] Ellipsometric measurements of the samples yielded an $Al_2O_3$ thickness of 0.75 nm. After the deposition of clusters (see below), one sample

* To whom correspondence should be addressed. E-mail: vajda@anl.gov.
[$] Present address: X-ray Sciences Division, Argonne National Laboratory, 9700 South Cass Avenue, Argonne, Illinois 60439.
[†] Chemical Sciences and Engineering Division, Argonne National Laboratory.
[‡] X-ray Sciences Division, Argonne National Laboratory.
[§] Materials Science Division, Argonne National Laboratory.
[||] Energy Systems Division, Argonne National Laboratory.
[⊥] Center for Nanoscale Materials, Argonne National Laboratory.
[#] Northwestern University.
[+] Present address: Materials Science Division, Argonne National Laboratory, 9700 South Cass Avenue, Argonne, Illinois 60439
[¶] Yale University.

10.1021/jp912220w © 2010 American Chemical Society
Published on Web 05/19/2010

was post-treated with a ~1 ML ALD-titania overcoat with the goal to alter surface chemistry and to suppress sintering of clusters during the course of the reaction. This process consisted of 6 cycles of $TiO_2$ ALD[27] of alternating exposures to titanium tetrachloride ($TiCl_4$) and $H_2O$, using 0.5 s reactant exposures and purge times of 60 s following the $TiCl_4$ and 120 s following the $H_2O$ at a deposition temperature of 50 °C. The amorphous alumina support and the titania-overcoated alumina support turned out to be inactive in the oxidative decomposition of methanol, in contrast to $\gamma$-alumina.[28]

**Size-Selected Cluster Deposition.** The size-selected palladium cluster-based catalysts were prepared by depositing a narrow size-distribution of palladium clusters generated in a laser vaporization cluster source. The size-selected cluster deposition method was described in detail elsewhere.[29−32] In brief, a molecular beam of palladium clusters was prepared by laser vaporization of a palladium target with helium as carrier gas. Then, the beam was guided through an ion optics and quadrupole assembly, and the mass-selected, positively charged clusters soft-landed on the support. The amount of deposited palladium metal was determined by real-time monitoring of the deposition flux. The surface coverage was 0.1 and 0.03 atomic ML equivalent of Pd metal for the $Pd_{8-12}$ and $Pd_{15-18}$ samples, respectively, based on $1.53 \times 10^{15}$ atoms/cm$^2$ of a Pd(111) plane. X-ray absorption (XANES) and X-ray photoelectron spectra (XPS) show that the clusters oxidized upon exposure to air. Before the reaction with methanol no treatment, such as reduction, was performed with the samples.

**Combined TPRx and in Situ GISAXS Characterization of Clusters.** GISAXS was used to monitor possible changes in cluster size during the reaction, simultaneously with monitoring catalyst activity by temperature-programmed reaction (TPRx). The GISAXS technique has proven to be very powerful for studying subnanometer- and nanometer-sized particles at surfaces and their transformations under vacuum conditions as well as in a reactive gas environment.[23,29−34] GISAXS is sensitive to the particles in the surface region, and in addition to the particle size. Therefore it can provide particle size distribution, distance between particles, and average aspect ratio of metal particles under reaction conditions. The GISAXS/TPRx experiments were performed by using X-rays of 12 keV energy in an in-house-built reaction cell of unique design at the 12-ID-C beamline of the Advanced Photon Source. The internal volume of the cell is approximately 25 mL, with the sample mounted on a ceramic heater in the center of the cell. The cell was sealed with mica windows and mounted on a computer-controlled goniometer and equipped with gas feedthroughs mounted in the side walls of the cell. The reactant gas mixture was premixed in a remotely controlled gas-mixing unit with calibrated mass flow controllers (Brooks model SLA5850). The reaction temperature was controlled with a ceramic heater, and the sample temperature was measured with a K-type thermocouple attached to the edge of the heater surface. To achieve thermal equilibrium between the heater and sample during the application of a temperature ramp, a low heating rate (<1.5 deg/min) was applied. The products were analyzed by using a differentially pumped mass spectrometer (Pfeiffer Prisma Plus).[23] The reaction cell was operated in a continuous gas flow mode at 800 Torr pressure and 30 mL min$^{-1}$ of total gas flow. Equal concentrations of methanol and oxygen in the feed were 0.33%; the concentration of water vapor was 50 ppm with the balance helium. The catalytic reactions were carried out at temperatures ranging from 25 to 250 °C. As illustrated in Figure 1, the X-ray beam was scattered off the surface of the sample at near the critical angle ($\alpha_c = 0.15°$) of the substrate. A 1024 × 1024 pixel two-dimensional detector was used for recording the GISAXS images from the sample. GISAXS data were collected as a function of reaction temperature and time.

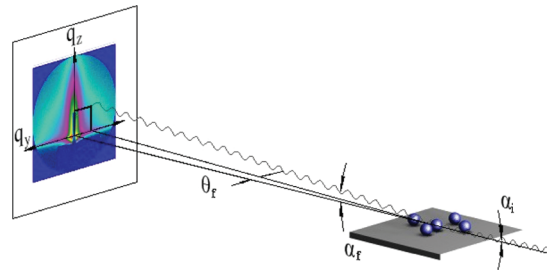


**Figure 1.** Schematic of GISAXS experiment: incident angle $\alpha_i = 0.15°$, and scattered beam angle $\alpha_f$. The two-dimensional scattering image provides information about the average height and width of a large ensemble of supported particles.

## Theoretical Methods

In a recent study, we have carried out a comprehensive density functional theory investigation of the pathways for methanol decomposition on a $Pd_4$ gas-phase cluster with more limited calculations done for a $Pd_8$ gas-phase cluster.[35] In the work reported here we have included the effects of the alumina support in the calculations on the $Pd_4$ and $Pd_8$ cluster as modeled by a $\theta$-$Al_2O_3$ surface. We have also considered the effect of CO loading on the reaction mechanism as CO poisoning may play an important role in the experimental results reported in this paper. The calculations performed in this study are based on density functional theory (DFT) with a plane-wave basis set, using the Vienna ab initio simulation package (VASP).[36,37] Ultrasoft pseudopotentials with a plane-wave energy cutoff of 400 eV were used with the generalized gradient correction of Perdew and Wang (GGA-PW91).[38] The geometries of the systems were determined by static relaxation, using a conjugate gradient minimization and the exact Hellmann−Feynman forces. The structures of gas-phase $Pd_4$ and $Pd_8$ clusters were fully optimized in 15 and 17 Å$^3$ supercell, respectively. These clusters were supported on a $\theta$-$Al_2O_3$ surface, which was modeled in a slab geometry with a (2 × 2) lateral periodicity. Six repeated $Al_2O_3$ layers were used to describe the surface, of which the three top layers were allowed to relax. The slabs were separated by a vacuum distance of 16 Å. A single *k*-point was used for the gas-phase cluster calculations, whereas the *k*-point sampling was performed with (3,3,1) Monkhorst−Pack grids[39] for surface calculations. The gas-phase Pd clusters and some of the gas-phase species have a magnetic moment, therefore spin-polarization was considered in all calculations.

## Results and Discussion

**$Pd_{8-12}/Al_2O_3$.** The conversion of methanol in the presence of oxygen and water vapor, studied over the $Pd_{8-12}/Al_2O_3$ sample, is shown in Figure 2. There are two distinct temperature regions with characteristic features seen in the plot: (1) a lower temperature region with onset of product formation around 130 °C and (2) a region above 200 °C with steep increase in reactivity. In the lower temperature range the major products identified were CO, $H_2O$, and $H_2$, with the addition of $CO_2$ and $CH_2O$ (formaldehyde) at temperatures above 200 °C. In addition, a small amount of $H_3C-O-CH_3$ (dimethyl ether, DME) was detected above 200 °C (see the insert in Figure 2). The most commonly reported methanol oxidative decomposition products

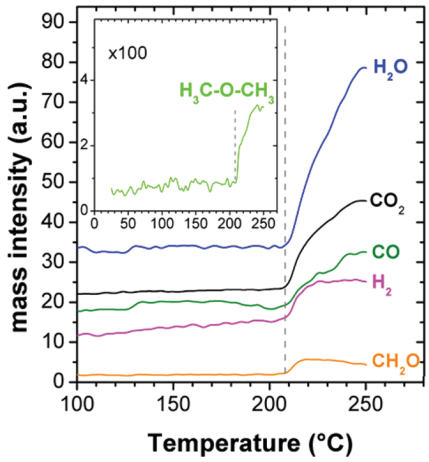


**Figure 2.** TPRx results of oxidative methanol decomposition on the 0.1 ML $Pd_{8-12}/Al_2O_3$ sample, with a reactant mixture of 0.33% $CH_3OH$, 0.33% $O_2$, and 50 ppm $H_2O$ vapor in He. The main reaction products identified were dimethyl ether (monitored at *m/z* 45), formaldehyde (*m/z* 30), CO (*m/z* 28), $CO_2$ (*m/z* 44), $H_2O$ (*m/z* 18), and $H_2$ (*m/z* 2). The signals plotted are background corrected, using a support of the same size and composition without catalytic particles, and tested under identical conditions as the catalyst-containing sample. For better viewing, offset was applied on the curves. For comparison of activities plotted in Figures 2 and 7, the scale for mass intensity shown is for *m/z* 30 (formaldehyde) relative to the mass intensity *m/z* 30 in Figure 7.

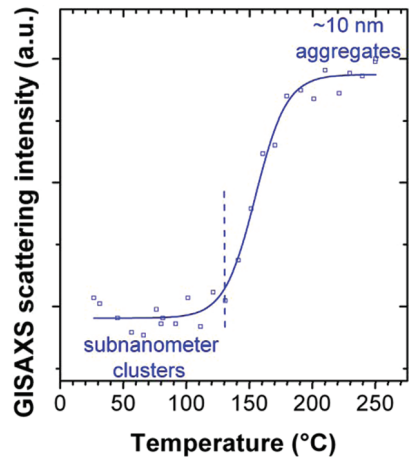


**Figure 3.** Integrated scattering intensities obtained from GISAXS images acquired during the reaction as a function of temperature. The data reveal the onset of sintering of the $Pd_{8-12}$ clusters at temperatures around 135 °C (dashed lines).

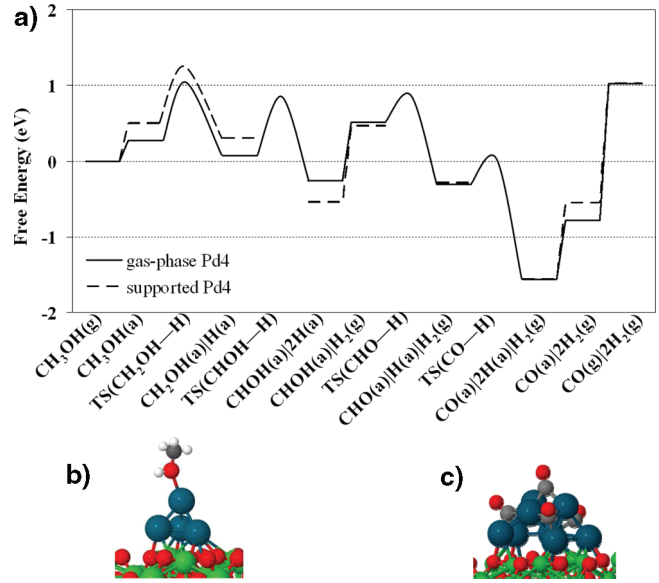


**Figure 4.** (a) Methanol decomposition pathway on $Pd_4$ leading to a strongly bound CO: free energy (calculated at 175 °C, 760 Torr) diagram for the lowest energy pathway for methanol decomposition on gas-phase $Pd_4$ cluster. Dotted lines are for selected steps calculated on the supported $Pd_4$ cluster. (b) Methanol adsorbed on the $Pd_4$ cluster on $Al_2O_3$ surface. (c) Four CO molecules adsorbed on a $Pd_8$ cluster on $Al_2O_3$ surface.

are $CO_2$, CO, and $H_2O$. The hydrogen signal exhibits a slow rise in the temperature region between ~100 and 200 °C. $H_2$ observed in the lower temperature region most likely indicates the recombination of dissociatively adsorbed hydrogen formed via methanol adsorption and subsequent decomposition.[9,12,14,35] CO formation is observed at 130 °C, followed by a slow decrease in its production with increasing temperature and extinguishes completely at 200 °C. The CO formation at lower temperatures provides evidence for the decomposition mechanism. Additional evidence for direct decomposition is provided by the increased production of $H_2$ and CO at higher temperatures. In addition, other methanol activation channels may contribute to hydrogen production as well, such as partial oxidation pathways yielding $CO_2$, $H_2O$, and formaldehyde in addition to hydrogen,[40] the latter which can be oxidized to produce $CO_2$ and $H_2$ as final products.[12,14,15] In passing we note that the production of some $H_2O$ in the low-temperature region, with an onset around 130 °C, does not necessarily contradict the proposed decomposition mechanism, since $H_2O$ is expected to be produced during the reduction of the oxidized Pd clusters and/or reaction of hydrogen with oxygen adsorbed on the surface of the Pd particles.

In situ GISAXS was applied to monitor possible changes in cluster size via sintering during the reaction. Since scattering intensity in the Guinier region ($q \times R_g < 1$)[34] is strongly size dependent (increases nonlinearly with the number of electrons in the particle, while the scattering intensity from particles of the same size, thus same number of electrons, scales with the number of particles), integrated scattering intensities in the small angle regions provide a very sensitive probe of the smallest changes in particle size without the need for demanding data analysis and modeling. Figure 3 shows the integrated GISAXS scattering intensity with a sharp increase at 135 °C, indicative of the onset of sintering. As determined by Guinier analysis[41] of the GISAXS patterns the sintering leads to the formation of ~10 nm aggregates at temperatures around 190 °C, without further aggregation with increasing temperature. It is noteworthy that the yield of all products exhibits a sharp increase at around 210 °C, a temperature that coincides with the well-known CO desorption temperature from metallic palladium particles and single crystal surfaces.[42,43] Thus, in the lower temperature region of our experiment the catalyst is very likely to be poisoned via CO adsorption blocking the adsorption sites.

Recently published UHV TPR CO oxidation experiments on size-selected Pd clusters of comparable sizes showed CO ligands departing from the clusters at temperatures around 180 °C,[44] in accord with the likelihood of CO poisoning based on our experimental observations and computational results.

The results from our density functional calculations for methanol decomposition on a $Pd_4$ cluster via C−H bond breaking as the first step are summarized in Figure 4. The figure shows our previously[35] calculated reaction pathway for a gas-phase cluster based on C−H bond breaking as the first step. The structure of methanol adsorbed on a $Pd_4$ cluster on $Al_2O_3$

**TABLE 1: CO and H Binding Energies on Gas-Phase and Supported $Pd_4$ and $Pd_8$ Clusters**

| cluster | binding energy (eV) | site[b] |
|---|---|---|
| $CO + Pd_4 \rightarrow (CO)Pd_4$ | −2.54 | H |
| $3CO + Pd_4 \rightarrow (CO)_3Pd_4$ | −2.00[a] | HBB |
| $CO + Pd_8 \rightarrow (CO)Pd_8$ | −2.36 | H |
| $CO + Pd_4/Al_2O_3 \rightarrow (CO)\ Pd_4/Al_2O_3$ | −2.31 | H |
| $4\ CO + Pd_4/Al_2O_3 \rightarrow (CO)_4Pd_4/Al_2O_3$ | −1.77[a] | HHHT |
| $CO + Pd_8/Al_2O_3 \rightarrow (CO)\ Pd_8/Al_2O_3$ | −2.33 | H |
| $3\ CO + Pd_8/Al_2O_3 \rightarrow (CO)_3Pd_8/Al_2O_3$ | −2.03[a] | HHH |
| $4\ CO + Pd_8/Al_2O_3 \rightarrow (CO)_4Pd_8/Al_2O_3$ | −1.87[a] | HHHH |

[a] Average value per CO molecule. [b] H = 3-fold hollow; B = bridge, T = top.

is shown in Figure 4b. Selected points for a $Pd_8$ gas-phase cluster gave similar results including the first step involving C−H bond breaking and the whole surface for C−O bond breaking.[35] Selected points along the $Pd_4$ cluster pathway were chosen for further study in this investigation with the alumina support included in the calculations. The results are included in Figure 4. The combination of the gas-phase and support results clearly show that the adsorption of CO results in a deep well that can poison the methanol decomposition reaction as is postulated to occur in the experiment.

To investigate the effect of multiple CO adsorptions on the $Pd_4$ and $Pd_8$ clusters, DFT calculations were performed for up to four COs on free and supported Pd clusters. Table 1 summarizes the average adsorbate binding energies as a function of the number of adsorbed CO molecules.

The structure of four adsorbed COs on a $Pd_8$ cluster is shown in Figure 4c. The results show that, at high CO coverage, the average binding energy decreased by 0.46 eV compared to that of the single CO adsorption. Thus, the binding energy for multiple CO adsorptions is still likely enough to poison the methanol decomposition reaction.

To obtain information about the possible poisoning of the catalyst, under assumption that competitive adsorption of hydrogen with CO may promote the desorption of reaction products, the experiment depicted in Figure 2 was continued at 250 °C and the feed of the reactants was stopped with a substitution by 1% hydrogen in helium. A very strong effect of hydrogen was observed: Immediately after the injection of hydrogen the partial pressure of the products increased by almost an order of magnitude (see Figure 5). The strong boost of products was observed only in a relatively short time window (∼5 min) due to the halted flow of reactants leading to the fast depletion of reactants and products in the cell.

In general, the significant increase in product signals on the 10 nm sized aggregates might be attributed to several pathways. One possibility is that hydrogen removes adsorbed oxygen and/or reduces palladium and boosts product formation by creating many more sites for methanol decomposition, the second is the reaction of hydrogen with $CH_x$ species adsorbed on the catalyst, and the third is a competitive adsorption of hydrogen with CO, leading to the unblocking of active sites. In the case of the decomposition channel, the mechanism involves the initial depletion of oxygen from the surface PdO by reaction with the introduced hydrogen, leading to the creation of a metallic Pd surface on the 10 nm size particles. Metallic Pd has been shown to be significantly more active than PdO for methanol decomposition.[7,12] The second possible explanation of the effect of added hydrogen is that adsorbed hydrogen on the 10 nm particles can react with adsorbed $CH_x$ species which are known to poison the methanol decomposition on Pd-based catalysts as

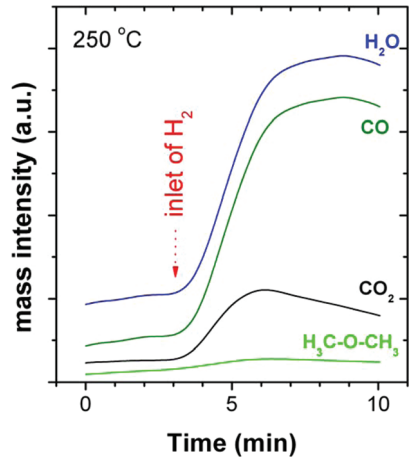


**Figure 5.** The effect of added hydrogen on the products from the sintered palladium catalyst of 10 nm average size at 250 °C. An offset was applied on the curves for clarity. The arrow indicates the time when the flow of reactant gases was halted and replaced by hydrogen seeded in He.

well.[12] Adsorbed $CH_x$ species are produced by breaking the C−O bond of methanol and are very stable up to about 187 °C, which results in inhibiting the reaction.[12] However, methane, which would be a product of this reaction path, was not detected under our reaction conditions. The third possible mechanism for the effect of hydrogen is promoting desorption of CO from the surface of the catalyst by competitive adsorption. Since the reaction temperature is 40 °C above the known desorption temperature of CO from palladium surfaces, it is reasonable to believe that the promotion effect of hydrogen via competitive adsorption does not play a decisive role.

Therefore, the apparent almost complete lack of activity of the $Pd_{8-12}/Al_2O_3$ sample in the lower temperature region is likely caused by CO poisoning. On the basis of in situ GISAXS, the observed reactivity data above 190 °C are attributed to 10 nm sized aggregates that are formed at elevated temperatures from the deposited size-preselected $Pd_{8-12}$ clusters. The most plausible effect of hydrogen in boosting the reaction at 250 °C is via the removal of adsorbed oxygen from the nanoparticles and reduction of the oxidized palladium nanoparticles.

**$Pd_{15-18}/Al_2O_3$ and Titania Overcoated $Pd_{15-18}/Al_2O_3$ ($TiO_2/Pd_{15-18}/Al_2O_3$).** To investigate the effect of size and support in the activation of methanol, $Pd_{15-18}$ clusters were deposited on an alumina support, and one of the cluster samples was post-treated by depositing ca. 1 ML of titania over the catalyst sample (Figure 6). Titania overcoating of $Pd/Al_2O_3$ catalysts was reported to achieve a higher dispersion of palladium.[45] In addition, titania can promote the reduction of PdO to metallic palladium,[45,46] further enhancing the efficacy of the decomposition channel. The titania overcoat may also improve the sintering resistance of the subnanometer clusters by forming a barrier around the clusters, as successfully demonstrated in the case of alumina-stabilized subnanometer gold clusters in the epoxidation of propylene.[17,19]

In comparison with the $Pd_{8-12}/Al_2O_3$ sample, the amount of deposited palladium metal in these samples was smaller by a factor of 3 in order to reduce aggregation by limiting particle diffusion. A significant enhancement in sintering resistance of the $Pd_{15-18}$ clusters was observed by GISAXS (Figure 6c). The onset of sintering by $Pd_{15-18}$ clusters supported on alumina was around 170 °C; an improvement in sintering resistance by 40 °C in comparison with the $Pd_{8-12}$ clusters (cf. Figure 3). After reaching 200 °C, sintering led to the formation of aggregates

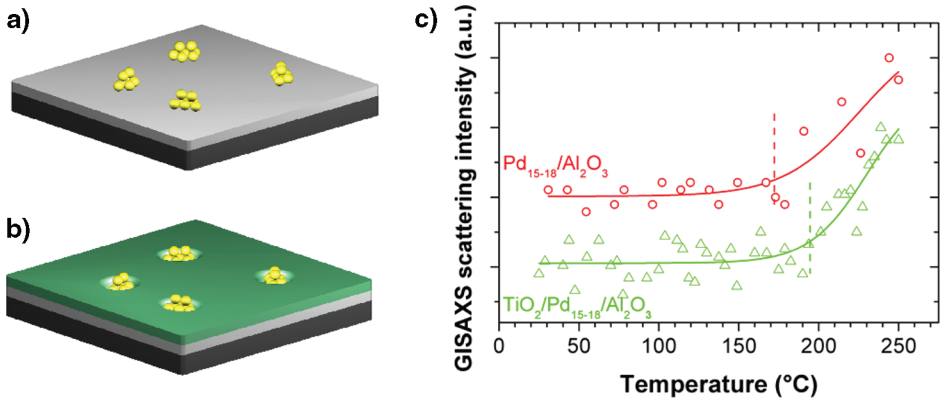


**Figure 6.** Cartoon of the $Pd_{15-18}/Al_2O_3$ (a) and titania overcoated cluster sample $TiO_2/Pd_{15-18}/Al_2O_3$ (b). Integrated GISAXS scattering intensities as a function of temperature for $Pd_{15-18}$ clusters without (circles) and with (triangles) titania protective overcoat (c), with an offset applied to the curves. The larger deviation of the data points obtained for the titania-ovecoated sample has its origin in the background scattering of the titania film.

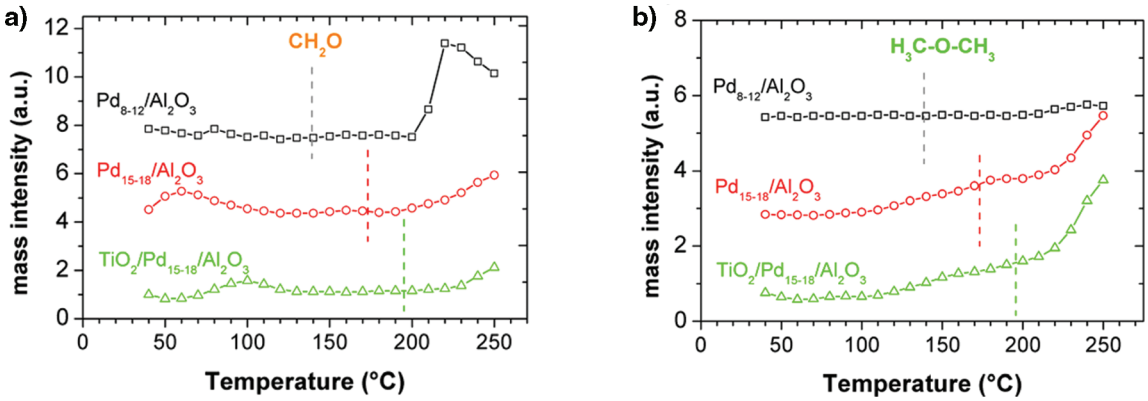


**Figure 7.** Evolution of the TPRx signals of $CH_2O$ (a) and DME (b) formed on $Pd_{15-18}/Al_2O_3$ (circles) and $TiO_2/Pd_{15-18}/Al_2O_3$ (triangles). The activity of the $Pd_{8-12}/Al_2O_3$ sample (squares) is shown for comparison. The background-corrected product signals are depicted with the identical scale and normalized to the number of atoms of the clusters to allow a per atom based comparison of activity for a given reaction product. An offset to the curves was applied for better viewing. The sintering temperatures are indicated with dashed vertical lines. The scale for the mass intensity was chosen based on $m/z$ of the $Pd_{8-12}/Al_2O_3$ sample.

of about 2 nm final sizes. The titania overcoated sample, $TiO_2/Pd_{15-18}/Al_2O_3$, exhibited a further enhanced stability during the reaction, with no indication of particle growth up to about 200 °C. The slight increase in scattering intensity observed at 210 °C (Figure 6c) could be an indication of aggregate formation to a degree that is much smaller than observed for $Pd_{8-10}$ (cf. Figure 3); however, this interpretation is by no means certain. Alternatively, reduced titania can migrate over the top of the Pd particles, due to strong metal−support interactions,[47] or form an interfacial alloy with palladium, which has been observed at temperatures as low as 25 °C.[48] The formation of such two-component particles can be reflected in GISAXS as a larger size particle. Moreover, titania islands may grow during the reaction and the scattering from these islands can interfere with the scattering from the metallic particles. Based solely on the available GISAXS data, it is not possible to unambiguously determine the type of species/aggregates that grow at temperatures above 210 °C on the titania overcoated $Pd_{15-18}$ sample. These nanostructures can be alloy and titania island scatterers formed in the course of the reaction as well as growing Pd particles.

The aggregation of Pd nanoparticles has been previously studied under ultrahigh vacuum conditions.[42,49] The mechanism of sintering has been explained by two different pathways, coalescence and Ostwald ripening. The relatively low temperature for the onset of agglomeration of the smaller Pd clusters, in our previous studies of sintering by subnanometer clusters,[50] as well as the generally higher mobility of smaller particles along with the high binding energies in atomic clusters suggest that particle coalescence is the dominant mechanism.

Figure 7 shows the activity of the $Pd_{15-18}$ clusters at temperatures lower than at which the sintering of clusters takes place with formation of dimethyl ether and formaldehyde. No detectable formation of CO, $CO_2$, and $H_2O$ was observed below the sintering temperature of the clusters. In passing, we note the low light-off temperature on the aggregating clusters compared to conventional catalysts.[7] It is important to note that $Pd_{8-12}$ clusters were not active in the lower temperature region under identical reaction conditions. Our results indicate that $Pd_{15-18}$ clusters are more resistant to poisoning than their smaller cousins. The activity and selectivity toward dimethyl ether formation at lower temperatures can be ascribed to the dehydration of methanol $2CH_3OH \rightarrow CH_3OCH_3 + H_2O$ as reported for alumina supported palladium catalysts.[51]

It is important to note that some forms of titania are active in the methanol decomposition reaction.[52,53] To investigate the potential catalytic activity of the monolayer titania film, we performed a control experiment in the absence of Pd using a titania overcoated alumina support of the same size and identical ALD-titania treatment as used for the overcoated Pd cluster

sample, and under identical reaction conditions. The catalytic activity of the titania-coated alumina was negligible, thus we can conclude that the primary role of the titania film is the stabilization of the clusters against sintering. Since there was no loss observed in the catalytic activity of the $TiO_2/Pd_{15-18}/Al_2O_3$ sample in comparison with the $Pd_{15-18}/Al_2O_3$ sample, it can be concluded that the active sites of the catalysts are not blocked (i.e., overcoated) by the titania film. The similarity in activity and selectivity for these catalysts implies that strong metal−support interactions are not operative. Indeed, this is expected for catalysts that have not been heated to the temperatures required for titania migration over the metal particles, i.e. 200−400 °C.[46] Moreover, the reactions were performed under oxidative conditions which might prevent the formation of the $Ti^{3+}$ oxidation state that is responsible for the SMSI effect especially under UHV and reduction conditions.

**Comparison of the Tested Catalysts: Size and Support Effects.** $Pd_{8-12}$ clusters produced primarily CO and $H_2$, while $Pd_{15-18}$ clusters produced $CH_2O$ and DME. The alumina-supported $Pd_{8-12}$ clusters showed the lowest activity among the tested catalysts due to poisoning. The very small amount of hydrogen and CO produced and the complete lack of dimethyl ether and formaldehyde formation in the lower temperature region (Figure 2) suggests that, at very low activity, $Pd_{8-12}$ clusters catalyze the decomposition channel. The almost complete lack of dimethyl ether formation indicates that the small clusters do not act as electron acceptors on the metallic part of the catalysts, thus they do not provide the Lewis acidic sites needed for the dehydration of alcohols.[54,55]

The behavior of $Pd_{15-18}$ clusters is diametrically different from that of their smaller counterparts; they are considerably more reactive, producing $CH_2O$ or DME, with high selectivity in the lower or higher temperature range, respectively (see Figure 7). At temperatures above 80 °C on alumina-supported $Pd_{15-18}$ clusters the formation of DME dominates, indicative of a Lewis acid character for these particles. The titania overcoat affects selectivity in the lower temperature region, where the formation of $CH_2O$ prevails (see Figure 7a). Very importantly, $Pd_{15-18}$ clusters proved to resist poisoning.[7] Moreover, the size-dependence of the oxidation behavior and the form of oxygen on palladium may play a critical role.[12]

## Conclusion

In summary, we have observed pronounced size and support effects in the oxidative decomposition of methanol on subnanometer palladium clusters. While $Pd_{8-12}$ clusters are susceptible to poisoning and decompose methanol with mediocre activity, $Pd_{15-18}$ clusters sustain activity in the decomposition of methanol to preferentially produce dimethyl ether. The thin titania overcoat improved the sintering-resistance of the clusters, without the catalysts suffering any loss in its activity, a central point for the production of new catalytic materials for applications. Though scaling up the production of ultrasmall clusters is a challenging task, there are several promising examples in the literature that indicate feasibility.[56,57]

**Acknowledgment.** The work at Argonne National Laboratory was supported by the U.S. Department of Energy, BES-Chemical Sciences, Materials Sciences, and BES-Scientific User Facilities under Contract DE-AC-02-06CH11357 with UChicago Argonne, LLC, Operator of Argonne National Laboratory. We gratefully acknowledge grants of computer time from EMSL, a national scientific user facility located at Pacific Northwest National Laboratory.

## References and Notes

(1) Iwasa, N.; Yamamoto, O.; Akazawa, T.; Ohyama, S.; Takezawa, N. *J. Chem. Soc., Chem. Commun.* **1991**, 1322.
(2) Chen, J. J.; Jiang, Z. C.; Zhou, Y.; Chakraborty, B. R.; Winograd, N. *Surf. Sci.* **1995**, *328*, 248.
(3) Holroyd, R. P.; Bowker, M. *Surf. Sci.* **1997**, *377−379*, 786.
(4) Chin, Y.-H.; Dagle, R.; Hu, J.; Dohnalkova, A. C.; Wang, Y. *Catal. Today* **2002**, *77*, 79.
(5) Cubeiro, M. L.; Fierro, J. L. G. *J. Catal.* **1998**, *179*, 150.
(6) Hoffmann, J.; Schauermann, S.; Johanek, V.; Hartmann, J.; Libuda, J. *J. Catal.* **2003**, *213*, 176.
(7) Matsumura, Y.; Shen, W.-J. *Top. Catal.* **2003**, *22*, 271.
(8) Bertarione, S.; Scarano, D.; Zecchina, A.; Johanek, V.; Hoffmann, J.; Schauermann, S.; Libuda, J.; Rupprechter, G.; Freund, H.-J. *J. Catal.* **2004**, *223*, 64.
(9) Kapoor, M. P.; Ichihashi, Y.; Nakamori, T.; Matsumura, Y. *J. Mol. Catal. A: Chem.* **2004**, *213*, 251.
(10) Rodriguez de la Fuente, O.; Borasio, M.; Galletto, P.; Rupprechter, G.; Freund, H. J. *Surf. Sci.* **2004**, *566−568*, 740.
(11) Libuda, J. *Surf. Sci.* **2005**, *587*, 55.
(12) Baumer, M.; Libuda, J.; Neyman, K. M.; Rosch, N.; Rupprechter, G.; Freund, H. J. *Phys. Chem. Chem. Phys.* **2007**, *9*, 3541.
(13) Fukuhara, C.; Kamata, Y.; Igarashi, A. *Appl. Catal., A* **2007**, *330*, 108.
(14) Borchert, H.; Jürgens, B.; Nowitzki, T.; Behrend, P.; Borchert, Y.; Zielasek, V.; Giorgio, S.; Henry, C. R.; Bäumer, M. *J. Catal.* **2008**, *256*, 24.
(15) Agrell, J.; Lindstrom, B.; Pettersson, L. J.; Jaras, S. G. Catalytic Hydrogen Generation from Methanol. *Catalysis* **2002**, *16*, 67.
(16) Rupprechter, G. *Catal. Today* **2007**, *126*, 3.
(17) Vajda, S.; Ballentine, G. E.; Mucherie, S.; Marshall, C. L.; Elam, J. W.; Pellin, M. J.; Lee, B.; Lo, C.-T.; Seifert, S.; Winans, R. E.; Calo, J. M. *Prepr. Pap.—Am. Chem. Soc., Div. Pet. Chem.* **2007**, *52*.
(18) Vajda, S.; Pellin, M. J.; Greeley, J. P.; Marshall, C. L.; Curtiss, L. A.; Ballentine, G. A.; Elam, J. W.; Catillon-Mucherie, S.; Redfern, P. C.; Mehmood, F.; Zapol, P. *Nat. Mater.* **2009**, *8*, 213.
(19) Lee, S.; Molina, L. M.; López, M. J.; Alonso, J. A.; Hammer, B.; Lee, B.; Seifert, S.; Winans, R. E.; Elam, J. W.; Pellin, M. J.; Vajda, S. *Angew. Chem., Int. Ed.* **2009**, *48*, 1467.
(20) Judai, K.; Wörz, A. S.; Abbet, S.; Heiz, U. *J. Am. Chem. Soc.* **2004**, *126*, 2732.
(21) Lee, S.; Fan, C.; Wu, T.; Anderson, S. L. *J. Chem. Phys.* **2005**, *123*, 124710.
(22) Herzing, A. A.; Kiely, C. J.; Carley, A. F.; Landon, P.; Hutchings, G. J. *Science* **2008**, *321*, 1331.
(23) Vajda, S.; Lee, S.; Sell, K.; Barke, I.; Kleibert, A.; von Oeynhausen, V.; Meiwes-Broer, K.-H.; Rodríguez, A. F.; Elam, J. W.; Pellin, M. J.; Lee, B.; Seifert, S.; Winans, R. E. *J. Chem. Phys.* **2009**, *131*, 121104.
(24) Ritala, M.; Leskela, M. Atomic Layer Deposition. In *Handbook of Thin Film Materials*; Nalwa, H. S., Ed.; Academic Press: San Diego, CA, 2001; Vol. 1, pp 103.
(25) Elam, J. W.; Groner, M. D.; George, S. M. *Rev. Sci. Instrum.* **2002**, *73*, 2981.
(26) Ott, A. W.; McCarley, K. C.; Klaus, J. W.; Way, J. D.; George, S. M. *Appl. Surf. Sci.* **1996**, *107*, 128.
(27) Ritala, M.; Leskela, M.; Nykanen, E.; Soininen, P.; Niinisto, L. *Thin Solid Films* **1993**, *225*, 288.
(28) Xu, M.; Lunsford, J. H.; Goodman, D. W.; Bhattacharyya, A. *Appl. Catal., A* **1997**, *149*, 289.
(29) Lee, B.; Seifert, S.; Riley, S. J.; Tikhonov, G.; Tomczyk, N. A.; Vajda, S.; Winans, R. E. *J. Chem. Phys.* **2005**, *123*, 74701.
(30) Winans, R. E.; Vajda, S.; Lee, B.; Riley, S. J.; Seifert, S.; Tikhonov, G. Y.; Tomczyk, N. A. *J. Phys. Chem. B* **2004**, *108*, 18105.
(31) Vajda, S.; Winans, R. E.; Elam, J. W.; Lee, B.; Pellin, M. J.; Seifert, S.; Tikhonov, G. Y.; Tomczyk, N. A. *Top. Catal.* **2006**, *39*, 161.
(32) Winans, R. E.; Vajda, S.; Ballentine, G. E.; Elam, J. W.; Lee, B.; Pellin, M. J.; Seifert, S.; Tikhonov, G. Y.; Tomczyk, N. A. *Top. Catal.* **2006**, *39*, 145.
(33) Vajda, S.; Wiederrecht, G. P.; Bouhelier, A.; Tikhonov, G. Y.; Tomczyk, N.; Lee, B.; Seifert, S.; Winans, R. E. *Collect. Czech., Chem. Commun.* **2007**, *72*, 121.
(34) Lei, Y.; Mehmood, F.; Lee, S.; Greeley, J. P.; Lee, B.; Seifert, S.; Winans, R. E.; Elam, J. W.; Meyer, R. J.; Redfern, P. C.; Teschner, D.; Schlögl, R.; Pellin, M. J.; Curtiss, L. A.; Vajda, S. *Science* **2010**, *328*, 224.
(35) Mehmood, F.; Greeley, J.; Curtiss, L. C. *J. Phys. Chem. C* **2009**, *113*, 21789.
(36) Kresse, G.; Furthmuller, J. *Phys. Rev. B* **1996**, *54*, 11169.
(37) Kresse, G.; Furthmuller, J. *Comput. Mater. Sci.* **1996**, *6*, 15.
(38) Perdew, J. P.; Chevary, J. A.; Vosko, S. H.; Jackson, K. A.; Pederson, M. R.; Singh, D. J.; Fiolhais, C. *Phys. Rev. B* **1992**, *46*, 6671.
(39) Monkhorst, H. J.; Pack, J. D. *Phys. Rev. B* **1996**, *13*, 5188.

(40) Gomes, J. R. B.; Gomes, J. A. N. F.; Illas, F. *J. Mol. Catal. A: Chem* **2001**, *170*, 187.

(41) Guinier, A.; Fournet, G.; Walker, C. B.; Yudowitch, K. L. *Small Angle Scattering of X-Rays*; Wiley: New York, 1955.

(42) Shaikhutdinov, S.; Heemeier, M.; Hoffmann, J.; Meusel, I.; Richter, B.; Bäumer, M.; Kuhlenbeck, H.; Libuda, J.; Freund, H.-J.; Oldman, R.; Jackson, S. D.; Konvicka, C.; Schmid, M.; Varga, P. *Surf. Sci.* **2002**, *501*, 270.

(43) Bertarione, S.; Scarano, D.; Zecchina, A.; Johánek, V.; Hoffmann, J.; Schauermann, S.; Frank, M. M.; Libuda, J.; Rupprechter, G.; Freund, H.-J. *J. Phys. Chem. B* **2004**, *108*, 3603.

(44) Kaden, W. E.; Wu, T.; Kunkel, W. A.; Anderson, S. L. *Science* **2009**, *326*, 826.

(45) Wang, C.-B.; Lin, H.-K.; Ho, C.-M. *J. Mol. Catal. A: Chem* **2002**, *180*, 285.

(46) Garcia, T.; Solsona, B.; Murphy, D. M.; Antcliff, K. L.; Taylor, S. H. *J. Catal.* **2005**, *229*, 1.

(47) Tauster, S. J. *Acc. Chem. Res.* **1987**, *20*, 389.

(48) Mikusik, P.; Bastl, Z. *Chem. Phys. Lett.* **1993**, *202*, 315.

(49) Jak, M. J. J.; Konstapel, C.; Kreuningen, A. v.; Chrost, J.; Verhoeven, J.; Frenken, J. W. M. *Surf. Sci.* **2001**, *474*, 28.

(50) Vajda, S.; Winans, R. E.; Elam, J. W.; Lee, B.; Pellin, M. J.; Riley, S. J.; Seifert, S.; Tikhonov, G.; Tomczyk, N. A. *Prepr. Pap.—Am. Chem. Soc., Div. Fuel Chem.* **2005**, *50*, 190.

(51) Iwasa, N.; Takezawa, N. *Top. Catal.* **2003**, *22*, 215.

(52) Kim, K. S.; Barteau, M. A. *Surf. Sci.* **1989**, *223*, 13.

(53) Farfan-Arribas, E.; Biener, J.; Friend, C. M.; Madix, R. J. *Surf. Sci.* **2005**, *591*, 1.

(54) Xu, M.; Goodman, D. W.; Bhattacharyya, A. *Appl. Catal., A* **1997**, *149*, 303.

(55) Licht, E.; Schächter, Y.; Pines, H. *J. Catal.* **1978**, *55*, 191.

(56) Argo, A. M.; Odzak, J. F.; Lai, F. S.; Gates, B. C. *Nature* **2002**, *415*, 623.

(57) Baldansuren, A.; Dilger, H.; Eichel, R. A.; van Bokhoven, J. A.; Roduner, E. *J. Phys. Chem C* **2009**, *113*, 19623.

JP912220W